かな左右差を認めた。

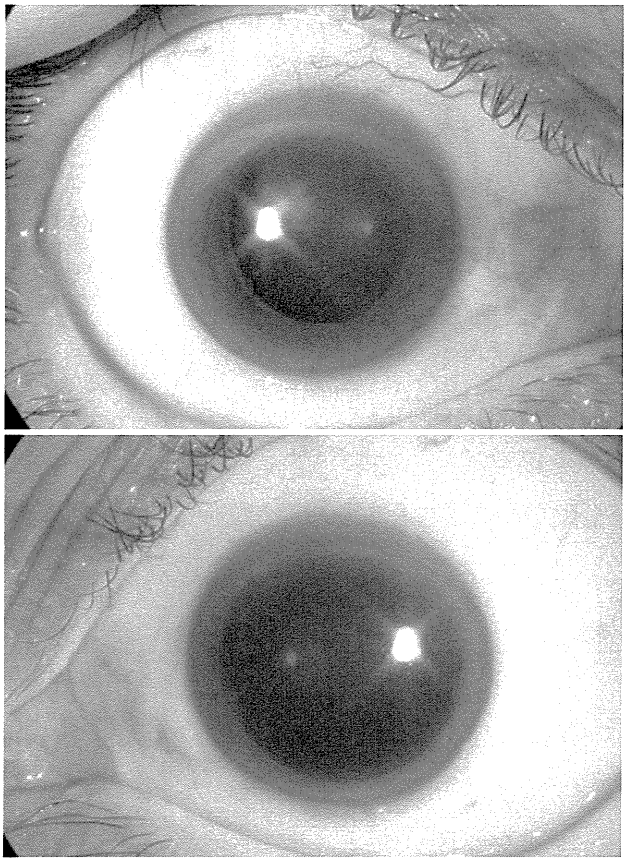

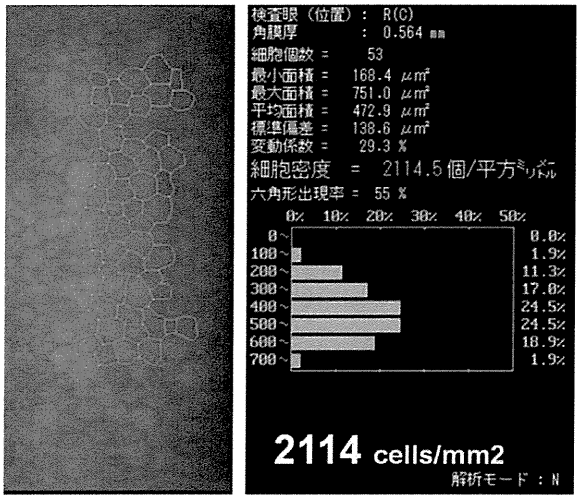

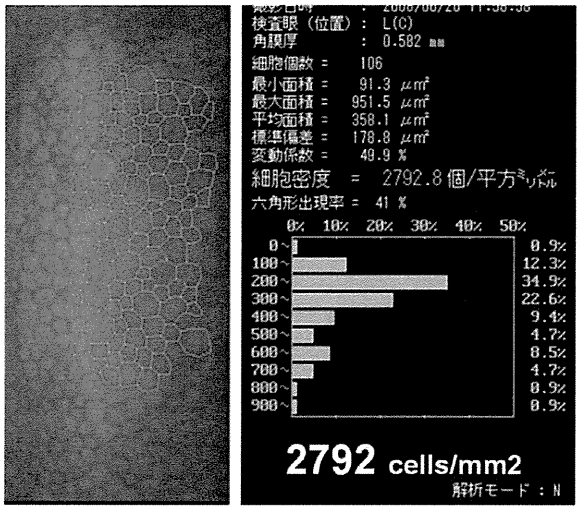

全体の結果を示す。患眼、瞭眼、対照眼における平均内皮細胞密度はそれぞれ 2288、2647、2774cells/mm^2 であり患眼は瞭眼、対照眼と比べて有意に角膜内皮細胞密度が低かった（p=0.0003、0.009）。瞭眼と対照眼に有意な差は認めなかった。

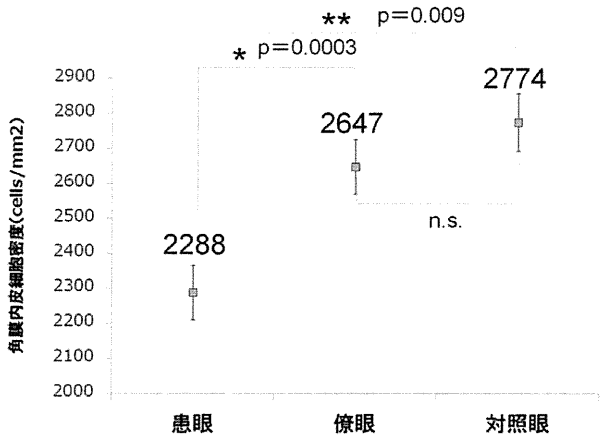

D. 考察

PEX における患眼では対照と比較して角膜内皮細胞密度が低下していることがわかった。我々の検討では、瞭眼については対照眼と有意な差は認めなかった。過去の報告では片眼性 PEX における瞭眼においても落屑物質の沈着が報告されている。

また、患眼、瞭眼ともに対照眼よりも角膜内皮細胞密度が低下している報告もあり、さらなる検討が必要と考える。

E. 結論

片眼性偽落屑症候群では患眼における角膜内皮細胞密度が低下する。

F. 研究発表（平成 23 年度）

論文発表　なし

学会発表　なし

著書・総説

1．相馬剛至、西田幸二：角膜内皮移植（DSAEK）DSAEK のドナー挿入法．「眼科手術」24 巻 4 号，401-403．2011

2．相馬剛至、西田幸二：角膜移植(眼球提供から移植まで)　ドナー検査と保存法．「眼科」　53 巻 12 号，1709-1713．2011．

その他：　なし

厚生労働科学研究費補助金（難治性疾患克服研究事業）
分担研究報告書

偽落屑角膜内皮症の実態把握と診断基準確立のための研究

研究分担者　布施　昇男　東北大学東北メガバンク機構ゲノム解析部門教授

研究要旨　現在我が国における緑内障有病率（40 歳以上）は約 5%とされ、その中でも失明になりやすい緑内障は落屑緑内障であり、手術介入をしても予後は不良である。今回 Toll-like receptor 4（*TLR4*）遺伝子、*CNTNAP2* 遺伝子において一塩基多型(SNP; single nucleotide polymorphism)をスクリーニングし、落屑緑内障と相関することを始めて明らかにした。今回の研究は、落屑緑内障と遺伝子の相関を解明する画期的なものであり、個人の疾患罹患率の予測や予防法の確立に向け、基礎的なデータとなる。

A. 研究目的

現在我が国における緑内障有病率(40 歳以上)は約 5%とされ，人口から概算して緑内障患者数は約 400 万人にものぼる。病型別に見てみると原発開放隅角緑内障の比率が高い。しかし、その中でも失明になりやすい緑内障は、落屑緑内障である。本邦において、落屑緑内障の分子遺伝学的な病態解明は急務の課題である。近年、*ゲノムワイドアソシエーションスタディ(GWAS)* を用いてその病態解析もされている。しかし、落屑緑内障と *LOXL1* 遺伝子と相関があると我々は報告している(Fuse N, et al. Mol Vis 2007)が、いまだ診断に応用できる感度にない。落屑緑内障の早期発見、発症前診断のために、免疫応答を担う Toll-like receptor 4 (*TLR4*) 遺伝子と神経ペプチド *CNTNAP2* 遺伝子をスクリーニングし、落屑緑内障と相関することを目的とした。

B. 研究方法

本研究では、東北大学病院眼科緑内障外来において収集した落屑緑内障患者標本を用い、各々 *TLR4* 遺伝子と *CNTNAP2* 遺伝子に焦点を絞り、スクリーニングを行った。*TLR4* 遺伝子上の 8 個の一塩基多型(SNP)rs10759930, rs1927914, rs1927911, rs12377632, rs2149356, rs11536889, rs7037117, rs7045953、*CNTNAP2* 遺伝子上の 8 個の SNP rs826802, rs1404699, rs7803992, rs700308, rs4725736, rs2107856, rs2141388, rs6970064 を選択し、プライマーを設定し、PCR 条件を設定した。PCR がスムーズに試行できていることを確認後、PCR ダイレクトシークエンス法にて、SNP をタイピングした。PCR は Takara Ex Taq® を用いて行い、PCR 断片は ExoSAP-IT® で精製、BigDye™ Terminator Cycle Sequencing Ready Reaction Kit でシークエンス反応を行った。シークエンサーは、ABI PRISM™ 3130 Genetic Analyzer を使用した。標本は、遺伝子型と表現型（臨床型）を後に解析できるように、臨床データがきちんと整備された貴重な標本である（落屑緑内障 90 例、正常対照 119 例）。塩基配列の確認は、DNA シーケ

ンスアセンブルソフトウェア SEQUENCHER™ を用いた。

（倫理面への配慮）

なおこの研究課題の計画にあたり、ヒトゲノム・遺伝子解析研究に関する倫理指針（平成 16 年文部科学省・厚生労働省・経済産業省告示第1号）に基づき、倫理委員会に緑内障遺伝子の解明のために東北大学眼科外来にてDNA検体を採取することについて申請しその承認を得てある。対象者に対する人権擁護上の配慮、研究方法による研究対象者に対する不利益、危険性の排除を十分考慮し、説明と同意（インフォームド・コンセント）を得た。

C. 研究結果

落屑緑内障と *TLR4* 遺伝子上の SNP に有意差を認めた。(rs1927914、rs1927911、rs12377632、rs2149356 のアリル頻度 p=0.019, 0.021, 0.038, 0.015, χ^2 テスト)。また、ハプロタイプ解析でも、p=0.014 と有意差を認め、落屑緑内障と *TLR4* 遺伝子に相関を認めた。（American Journal Ophthalmology, in revision）また、落屑緑内障と *CNTNAP2* 遺伝子上の SNP に有意差を認めた。(rs1404699, rs7803992 のアリル頻度 p=0.0086, 0.00054, χ^2 テスト) また、ハプロタイプ解析でも、p=0.004 と有意差を認め、落屑緑内障と *CNTNAP2* 遺伝子に相関を認めた。 (Molecular Vision, submitted)

D. 考察

TLR ファミリーは、自然免疫機構で中心的な役割を果たし、外因性のリガンドを認識し自己、非自己を区別するパターン認識受容体である。今回有意だった SNP は mRNA の安定性に関与し *TLR4* 遺伝子発現に影響を与えている可能性がある。ある種の慢性の感染や炎症が落屑緑内障の発症を誘発しうると推測された。*CNTNAP2* 遺伝子は、神経ペプチドであり、上皮増殖因子、ラミニン・グロブラードメイン等を介し、細胞接着、遊走等に関係しているとされる。今回有意だった SNP は上記ドメインの近くに存在し、細胞接着、遊走等に影響を与え、落屑緑内障の発症に関連していると推測された。

E. 結論

TLR4 遺伝子の SNP rs1927914、rs1927911、rs12377632、rs2149356、*CNTNAP2* 遺伝子の SNP rs1404699, rs7803992 が各々落屑緑内障と相関する。

F. 研究発表（平成 23 年度）

学会発表

布施昇男：緑内障の遺伝子診断の潮流
第 120 回青森眼科集談会、弘前、2011.4.24

高野良真、石棟、中澤徹、西田幸二、布施昇男：正常眼圧緑内障における *TLR4* 遺伝子の評価
第 115 回日本眼科学会総会、東京、2011.5.12

布施昇男：緑内障個別化医療に向けた遺伝子解析
第 3 回 KEEP THE VISUAL FIELD、熊本、2011.6.19

高野良真、石棟、清水愛、中澤徹、布施昇男：開放隅角緑内障、偽落屑症候群における*TLR4*遺伝子の評価　第22回日本緑内障学会、秋田、2011.9.23

厚生労働科学研究費補助金（難治性疾患克服研究事業）
分担研究報告書

偽落屑症候群における角膜内皮細胞密度の検討

研究分担者　宮田和典　　宮田眼科病院

研究要旨　偽落屑症候群（pseudoexfoliation syndrome , PE）は、虹彩、水晶体、チン氏帯など眼内組織に偽落屑物質が付着し、時には水晶体偏位や続発性緑内障を合併することもある。内眼手術に際しても、チン氏帯断裂など術中に合併症が生じやすい疾患である。また、近年ではPEにおける角膜内皮細胞の減少が報告されている。

A. 研究目的

偽落屑症候群（pseudoexfoliation syndrome ,PE）における角膜内皮細胞密度を検討すること。

B. 研究方法

細隙灯顕微鏡検査で、散瞳後にPEの有無を判定した。PEを認める患者93例115眼をPE群（平均年齢78.4±6.7歳）、年齢をマッチさせたPEがない患者100例120眼（78.2±5.5歳）を正常対照群とし、両群で比較検討した。また、同一患者で、片眼がPEで他眼にPEがない34眼（77.5±6.6歳）を、それぞれPE(+)とPE(−)とし、両眼を比較した。角膜内皮細胞密度をPE群と正常対照群、PE(+)とPE(−)で比較検討した。角膜細胞密度検査はスペキュラーマイクロスコピーを使用した。眼内手術既往例および緑内障は対象外とした。

（スペキュラーマイクロスコピー検査は、非侵襲的であり、検査を行うことによる患者への不利益は生じない。）

C. 研究結果

角膜内皮細胞密度はPE群、正常対照群でそれぞれ 2458±419/mm2、2633±258/mm2 であり、PE群において、正常対照群より有意な減少を認めた（* $p<0.05$, Mann-Whitney's U test）（図1）。また、PE(+)と PE(−)では、それぞれ 2517±278/mm2、2584±233/mm2 であり、統計学的有意差は認めなかったが（*Wilcoxon* signed-rank test）、PE(+)はPE(−)よりも減少傾向ではあった（図2）。

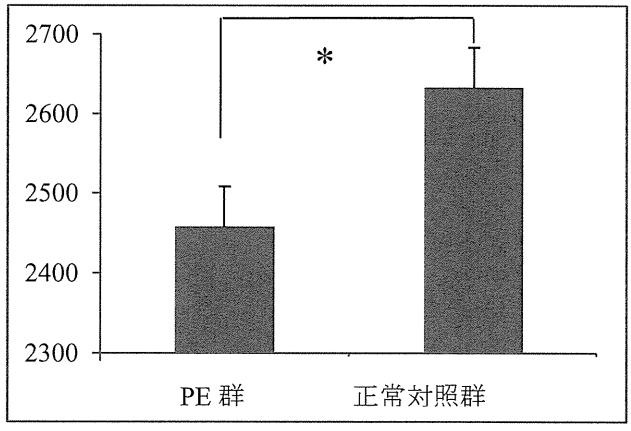

図1

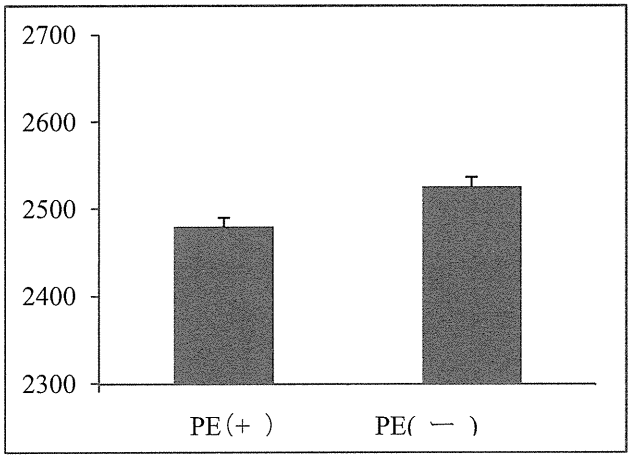

図 2

D. 考察

PE では角膜内皮細胞数の減少が認められた。現在のところ、偽落屑物質と角膜内皮減少との関連については不明である。偽落屑物質が角膜組織への何らかの作用により、角膜内皮細胞の変化が生じる可能性が考えられる。

E. 結論

偽落屑症候群では、正常眼と比較して角膜内皮細胞密度の減少を認めた。

F．研究発表（平成 23 年度）

論文発表

1. Miyanaga M、Sugita S、Miyata K et al; A significant association of viral loads with corneal endothelial cell damage in cytomegalovirus anterior uveitis. Br J Ophthalmol. 2010, 94(3)336-340,

学会発表

１．鄭暁東、宮田和典、大橋裕一ら 水疱性角膜症に対する角膜移植の多施設サーベイランス：病因と術式の検討 第 36 回角膜カンファランス・第 28 回日本角膜移植学会

G. 知的所有権の取得状況

(エ) 特許取得：なし

(オ) 実用新案登録：なし

(カ) その他：なし

研究成果の刊行に関する一覧表

雑誌

発表者氏名	論文タイトル名	発表誌名	巻号	ページ	出版年
Zheng X, Shiraishi A, Okuma S, Mizoue S, Goto T, Kawasaki S, et al.	In vivo confocal microscopic evidence of keratopathy in patients with pseudoexfoliation syndrome.	Invest Ophthalmol Vis Sci.	52	1755-61	2011
Zheng X, Sakai H, Goto T, Namiguchi K, Mizoue S, Shiraishi A, Sawaguchi S, Ohashi Y	Anterior Segment Optical Coherence Tomography Analysis of Clinically Unilateral Pseudoexfoliation Syndrome: Evidence of Bilateral Involvement and Morphological Factors Related to Asymmetry.	Invest Ophthalmol Vis Sci.	52(8)	5679-84	2011
Hatou S, Shimmura S, Shimazaki J, Usui T, Amano S, Yokogawa H, Kobayashi A, Zheng X, Shiraishi A, Ohashi Y, Inatomi T, Tsubota K	Mathematical projection model of visual loss due to fuchs corneal dystrophy.	Invest Ophthalmol Vis Sci.	52(11)	7888-93	2011
Miyazaki D, Haruki T, Takeda S, Sasaki S, Yakura K, Terasaka Y, Komatsu N, Yamagami S, Touge H, Touge C & Inoue Y	Herpes simplex virus type 1-induced transcriptional networks of corneal endothelial cells indicate antigen presentation function.	Invest Ophthalmol Vis Sci	52	4282-93	2011
Takeda S, Miyazaki D, Sasaki S, Yamamoto Y, Terasaka Y, Yakura K, Yamagami S, Ebihara N, & Inoue Y	Roles played by toll-like recetor-9 in corneal endothelial cells after herpes simplex virus type 1 infection.	Invest Ophthalmol Vis Sci	52	6729-36	2011
Nakatsukasa M, Sotozono C, Shimbo K, Ono N, Miyano H, Okano A, Hamuro J, Kinoshita S.	Amino Acid profiles in human tear fluids analyzed by high-performance liquid chromatography and electrospray ionization tandem mass spectrometry.	Am J Ophthalmol.	151(5)	799-808. el.	2011
Higa A, Sakai H, Sawaguchi S, Iwase A, Tomidokoro A, Amano S, Araie M	Prevalence of and risk factors for cornea guttata in a population-based study in a southwestern island of Japan. The Kumejima study.	Arch Ophthalmol	129	332-336	2011

Hotehama A, Mimura T, Usui T, Kawashima H, Amano S	Sudden onset of amantadine-induced reversible bilateral corneal edema in an elderly patient: Case report and literature review.	Jpn J Ophthalmol	55	71-74	2011
相馬剛至、西田幸二	角膜内皮移植（DSAEK）DSAEKのドナー挿入法.	「眼科手術」	24巻 4号	401-403	2011
相馬剛至、西田幸二	角膜移植(眼球提供から移植まで) ドナー検査と保存法.	「眼科」	53巻 12号	1709-13	2011
Miyanaga M、Sugita S、Miyata K et al	A significant association of viral loads with corneal endothelial cell damage in cytomegalovirus anterior uveitis.	Br J Ophthalmol.	94(3)	336-340	2010

In Vivo Confocal Microscopic Evidence of Keratopathy in Patients with Pseudoexfoliation Syndrome

Xiaodong Zheng,[1] *Atsushi Shiraishi,*[1] *Shinichi Okuma,*[1] *Shiro Mizoue,*[1] *Tomoko Goto,*[1,2] *Shiro Kawasaki,*[1] *Toshihiko Uno,*[1,3] *Tomoko Miyoshi,*[1,2] *Alfredo Ruggeri,*[4] *and Yuichi Ohashi*[1]

Purpose. To measure the density of cells in different layers of the cornea and to determine whether morphologic changes of the subbasal corneal nerve plexus are present in eyes with the pseudoexfoliation (PEX) syndrome.

Methods. Twenty-seven patients with unilateral PEX syndrome and 27 normal controls were investigated. All eyes underwent corneal sensitivity measurements with an esthesiometer and in vivo confocal microscopic study. Densities of the epithelial, stromal, and endothelial cells were measured. The density and tortuosity of the subbasal corneal nerve plexus were also evaluated.

Results. Eyes with PEX syndrome had significantly lower cell densities in the basal epithelium ($P = 0.003$), anterior stroma ($P = 0.007$), intermediate stroma ($P = 0.009$), posterior stroma ($P = 0.012$), and endothelium ($P < 0.0001$) than in the corresponding layers of normal eyes. PEX eyes also had lower subbasal nerve densities and greater tortuosity of the nerves than normal eyes. Fellow eyes of patients with PEX also had significantly lower densities of the basal epithelial and endothelial cells than the normal eyes. Corneal sensitivity was significantly decreased in PEX eyes, and this was significantly correlated with the decrease of basal epithelial cell and subbasal nerve densities.

Conclusions. These results have shed light on understanding of the pathogenesis of decreased corneal sensitivity in eyes with PEX syndrome. PEX syndrome is probably a binocular condition for which keratopathy of the fellow eye also requires observation. (*Invest Ophthalmol Vis Sci.* 2011;52:1755–1761) DOI:10.1167/iovs.10-6098

The pseudoexfoliation (PEX) syndrome is a common age-related disorder of the extracellular matrix and is frequently associated with severe chronic secondary open angle glaucoma and cataract.[1–3] The prevalence of PEX syndrome varies widely in different racial and ethnic populations. In addition, the prevalence of PEX is dependent on the age and sex distribution of the population examined, the clinical criteria used to diagnose PEX, and the ability of the examiner to detect early stages and more subtle signs of PEX. For example, the highest rates in studies of persons older than 60 years of age have been reported to be approximately 25% in Iceland and more than 20% in Finland.[3,4] The ocular manifestation of PEX syndrome is the production and progressive accumulation of abnormal extracellular fibrillar material in almost all the inner wall tissues of the anterior segment of the eye. This characteristic alteration predisposes the eye to a broad spectrum of intraocular complications including phacodonesis and lens subluxation, angle closure glaucoma, melanin dispersion, poor mydriasis, blood-aqueous barrier dysfunction, posterior synechiae, and other related complications.[1–3]

The PEX syndrome is associated with corneal endotheliopathy, and this has been suggested to be the cause of the so-called atypical non-guttata Fuchs endothelial dystrophy.[5,6] PEX endotheliopathy, a slowly progressing disease of the corneal endothelium, is usually bilateral but is often asymmetrical. It can lead to early corneal endothelial cell decompensation, which can then induce severe bullous keratopathy, a vision-threatening disorder.

Clinical signs of PEX syndrome include decreased corneal sensitivity, thinning of the central corneal thickness, and impaired tear film stability.[7–9] However, the underlying cause of these clinical findings has not been well investigated, possibly because objective and accurate in vivo examination techniques are not available.

Recent advances in imaging technology have improved the ability of these instruments to diagnose different ocular diseases. The Rostock Cornea Module (Heidelberg Engineering, Heidelberg, Germany), consisting of a contact lens system attached to the Heidelberg Retina Tomograph II (Heidelberg Engineering), is such an instrument. It uses laser scanning technology to investigate the cornea at a cellular level, and structures such as the subbasal nerve plexus, which cannot be seen by slit-lamp microscopy, can be clearly seen.[10,11]

In vivo confocal microscopy (IVCM) was used by Martone et al.[12] to examine one eye with PEX syndrome, and noncontact IVCM was used by Sbeity et al.[13] to study PEX, PEX-suspect, and normal eyes. However, there has not been a detailed and quantitative study of the morphologic changes in the corneas of eyes with PEX syndrome.

Thus, the purpose of this study was to examine the underlying pathogenesis of PEX keratopathy and to obtain evidence to explain clinical findings such as the decreased corneal sensitivities observed in patients with PEX syndrome. To accomplish this, we used IVCM to determine cell densities in different corneal layers of eyes with PEX syndrome and their clinically unaffected fellow eyes. These findings were compared with those in normal control eyes. The nerve densities in the subbasal layer were also analyzed, and their relationship with the alterations of clinical corneal sensitivity were analyzed.

From the [1]Department of Ophthalmology, Ehime University School of Medicine, Ehime, Japan; [2]Department of Ophthalmology, Takanoko Hospital, Ehime, Japan; [3]Department of Ophthalmology, Red Cross Hospital in Matsuyama, Ehime, Japan; and [4]Department of Information Engineering, University of Padua, Padua, Italy.

Submitted for publication June 22, 2010; revised October 8, 2010; accepted November 1, 2010.

Disclosure: **X. Zheng**, None; **A. Shiraishi**, None; **S. Okuma**, None; **S. Mizoue**, None; **T. Goto**, None; **S. Kawasaki**, None; **T. Uno**, None; **T. Miyoshi**, None; **A. Ruggeri**, None; **Y. Ohashi**, None

Corresponding author: Xiaodong Zheng, Department of Ophthalmology, Ehime University School of Medicine, Toon City, Ehime 791-0295, Japan; xzheng@m.ehime-u.ac.jp.

Subjects and Methods

Subjects

We studied 27 patients (16 men, 11 women; mean age, 74.4 ± 6.3 years; age range, 65–90 years) with diagnoses of unilateral PEX syndrome. In all eyes, exfoliation material (XFM) was seen by slit-lamp microscopy at the pupillary border or on the anterior lens capsule. Eyes with PEX syndrome were placed in the PEX group, and clinically normal fellow eyes were placed in the PEX fellow eye group. Age- and sex-matched normal subjects (16 men, 11 women; mean age, 72.7 ± 6.5 years; age range, 61–92 years) were also studied. One eye from the normal control group was randomly selected and used in the statistical analyses. Exclusion criteria included Stevens-Johnson syndrome, lymphoma, sarcoidosis, corneal dystrophy, injury, inflammation, systemic therapy with drugs with known corneal toxicity; treatment with topical anti-glaucoma drugs, steroids, or NSAIDs; contact lens wear; previous ocular surgery; and other ophthalmic diseases.

The procedures used conformed to the tenets of the Declaration of Helsinki. Informed consent was obtained from all subjects after an explanation of the nature and possible consequences of the procedures. The protocol used was approved by the Ethics Committee of Ehime University School of Medicine.

Corneal Sensitivity Measurements

Measurement of the corneal sensitivity was performed with a Cochet-Bonnet nylon thread esthesiometer, as described.[14] The examination was begun with a 60-mm length of nylon filament applied perpendicularly to the central cornea, and the tests were continued by shortening the filament by 5 mm each time until the subject felt the contact of the filament. Each subject was measured twice with a between-test interval of at least 5 minutes, and the average of two measurements was used for the statistical analyses.

In Vivo Confocal Microscopy

IVCM was performed on all subjects with the Rostock Corneal Module of the Heidelberg Retina Tomograph II (HRTII-RCM; Heidelberg Engineering). After topical anesthesia with 0.4% oxybuprocaine (Santen Pharmaceuticals, Osaka, Japan), the subject was positioned in the chin and forehead holder and instructed to look straight ahead at a target to make sure that the central cornea was scanned. The objective of the microscope was an immersion lens (magnification ×63; Zeiss, Chester, VA) covered by a polymethylmethacrylate cap (TomoCap; Heidelberg Engineering). Comfort gel (Bausch & Lomb, Berlin, Germany) was used to couple the applanating lens cap to the cornea. The polymethylmethacrylate cap was applanated onto the center of the cornea by adjusting the controller, and in vivo digital images of the cornea were seen on the monitor screen. When the first layer of superficial epithelial cells was seen, the digital micrometer gauge was set to zero, and then a sequence of images was recorded as the focal plane was gradually moved toward the endothelium. Each subject underwent scanning three times at intervals of at least 15 minutes.

The laser source of the HRT-II RCM is a diode laser with a wavelength of 670 nm. Two-dimensional images consisting of 384 × 384 pixels covering an area of 400 × 400 μm were recorded. The digital resolution was 1.04 μm/pixel transversally and 2 μm/pixel longitudinally, as stated by the manufacturer.

Image Analyses

Central corneal images of all subjects were taken, and the three best-focused images from the superficial epithelium, basal epithelium, subbasal nerve plexus, anterior stroma, intermediate stroma, posterior stroma, and endothelium were selected for analyses. The selected images were randomly presented to two masked observers (XZ, SO) for evaluation. All data are presented as averages of three images.

Cell Density Analyses

Morphologic characteristics and densities in the different layers of the cornea in the PEX and PEX fellow eyes were assessed and compared with those of normal controls. Superficial epithelial cells were identified as polygonal cells with clearly visible cell borders, bright cytoplasm, and dark nuclei. Basal epithelial cells were identified as the layer just above the amorphous-appearing Bowman membrane. Basal cells had bright borders, a uniform shape, and nonhomogeneous cytoplasm. The anterior stroma was identified as the first layer immediately beneath the Bowman membrane, and the posterior stroma was identified as the layer just anterior to the Descemet membrane and the endothelium. The intermediate stroma was defined as the layer halfway between the anterior and posterior stroma.[15] The corneal endothelium consisted of a monolayer of regularly arranged hexagonal cells with dark borders and bright reflecting cytoplasm.

After selecting a frame of the image and manually marking the cells inside the frame (>50 cells), cell densities were calculated automatically by the software installed in the instrument. Cells partially contained in the area analyzed were counted only along the upper and right margins. The results are expressed in cells per square millimeter.

Analyses of Subbasal Nerve Plexus

The subbasal nerve plexus layer is located between the Bowman membrane and the basal epithelial layer through which numerous nerve fibers pass. The density and tortuosity of the subbasal nerve plexus were analyzed as described.[14,16] Two parameters were analyzed: the long nerve fiber density (LNFD) was determined by dividing the number of long nerves by the image area (0.16 mm^2), and the nerve branch density (NBD) was determined by dividing the total number of long nerves and their branches by the image area. Nerve tortuosity was classified into 4 gradings: grade 1 = approximately straight nerves; grade 4 = very tortuous nerves with significant convolutions throughout their course.[16]

Statistical Analyses

Data were analyzed with statistical software (JMP, version 8.0 for Windows; SAS Japan Inc., Tokyo, Japan). All data are expressed as the mean ± SD. The differences of cell densities between PEX eyes and normal controls or between PEX fellow eyes and normal controls were evaluated with two-tailed Student's *t*-tests. The differences of cell densities between PEX eyes and their fellow eyes were evaluated by paired *t*-tests. The Wilcoxon rank sum test was used to compare the values of corneal sensitivity, LNFD, NBD, and the nerve tortuosity between PEX patients and normal controls. Spearman's correlation was used to determine the correlation among the parameters of basal epithelial cell density, subbasal nerve density, and corneal sensitivity. $P < 0.05$ was considered statistically significant.

Results

The mean age was not significantly different between patients with PEX and normal controls (two-tailed Student's *t*-tests, $P = 0.725$). Eyes with PEX showed typical whitish exfoliation material on the pupillary border or on the anterior lens capsule on slit-lamp examination. Pigmented keratoprecipitates and slight folding of Descemet membrane were also detected in some patients. Fellow eyes of PEX eyes and normal control eyes appeared normal by slit-lamp microscopy.

Corneal Sensitivity

The mean corneal sensitivity was 47.8 ± 5.6 mm for PEX eyes and 53.7 ± 4.9 mm for PEX fellow eyes. This difference was significant ($P = 0.005$; Wilcoxon rank sum test). Mean corneal

sensitivity was 55.6 ± 4.7 mm for the normal control subjects, and the corneas of eyes with PEX were significantly less sensitive than those of normal control eyes ($P < 0.0001$). The difference in corneal sensitivity between PEX fellow eyes and normal controls was not significant ($P = 0.378$).

Cell Densities

The density of the corneal superficial epithelial cells was 872.6 ± 95.3 cells/mm^2, and that for the basal epithelial cells was 4829.7 ± 462.1 cells/mm^2 in PEX eyes. Densities for the corresponding layers in PEX fellow eyes were 910.4 ± 80.8 cells/mm^2 and 4996.7 ± 438.7 cells/mm^2, and densities for the normal control eyes were 886.4 ± 101.7 cells/mm^2 and 5446.4 ± 639.9 cells/mm^2. The density of the basal epithelial cells was significantly lower for PEX eyes and PEX fellow eyes than for the control eyes ($P = 0.003$ and $P = 0.015$, respectively; two-tailed Student's *t*-tests; Fig. 1). The difference in the density of the basal epithelial cells between PEX eyes and PEX fellow eyes was not significant ($P = 0.589$; paired *t*-test). Differences in the densities of the superficial epithelial cells among the three experimental groups also were not significant (Fig. 1).

Densities of the cells in the three stromal layers of PEX eyes, PEX fellow eyes, and normal control eyes are shown in Figure 2. Compared with normal controls, the cell densities of PEX eyes were significantly lower in all three layers of the stroma (anterior stroma, $P = 0.007$; intermediate stroma, $P = 0.009$; posterior stroma, $P = 0.012$; two-tailed Student's *t*-tests). The densities in these three stromal layers in PEX fellow eyes were also lower, but the decrease was not significant ($P = 0.196$; $P = 0.261$; $P = 0.08$; respectively; Fig. 2).

Endothelial cell densities were 2240.7 ± 236.6 cells/mm^2, 2386.6 ± 200.8 cells/mm^2, and 2738.7 ± 233.2 cells/mm^2 for PEX eyes, PEX fellow eyes, and normal eyes, respectively. Differences between PEX eyes and normal controls ($P < 0.0001$; two-tailed Student's *t*-test; Fig. 1) and between PEX fellow eyes and normal controls were significant ($P = 0.001$). The difference in endothelial cell density between PEX and PEX fellow eyes was not significant ($P = 0.754$; paired *t*-test).

There was a higher degree of pleomorphism and polymegethism in PEX eyes than in control eyes. The coefficient of variation (CV) of the cell area was 45.2% ± 8.7%, and the percentage of hexagonal cells (HEX) in PEX eyes was 30.5% ± 10.3%. Both values are significantly different from those of normal control eyes (CV, 30.6% ± 5.6%, $P = 0.016$; HEX, 50.3 ± 6.8%, $P = 0.008$; two-tailed Student's *t*-test). PEX fellow eyes also showed a similar tendency of increased pleomorphism and polymegethism, but the differences were not statistically significant.

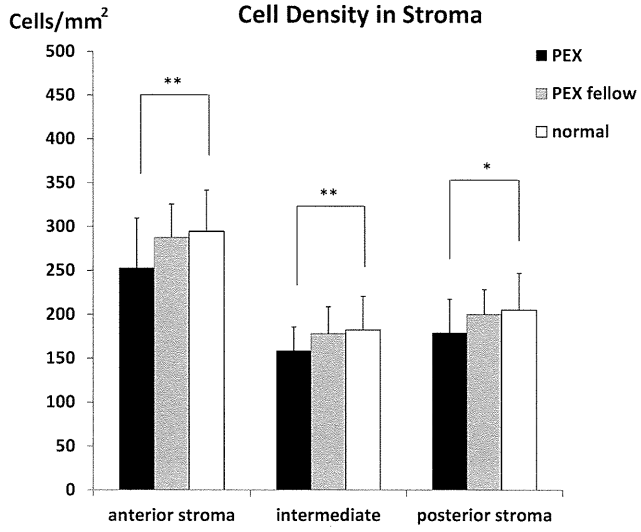

FIGURE 2. Cellular densities of anterior, intermediate and posterior stroma of eyes with PEX syndrome, their clinically unaffected fellow eyes, and eyes of normal control subjects. $^{**}P < 0.01$; $^{*}P < 0.05$.

Subbasal Nerve Plexus

The LNFD and NBD were significantly decreased in PEX eyes (17.4 ± 6.3 and 32.2 ± 8.3 nerves/mm^2, respectively) compared with those in normal controls (35.9 ± 8.2 and 72.2 ± 8.8 nerves/mm^2; $P < 0.0001$ and $P < 0.0001$, respectively; Wilcoxon rank sum test; Fig. 3). PEX fellow eyes also had decreased LNFD and NBD, but these changes were not

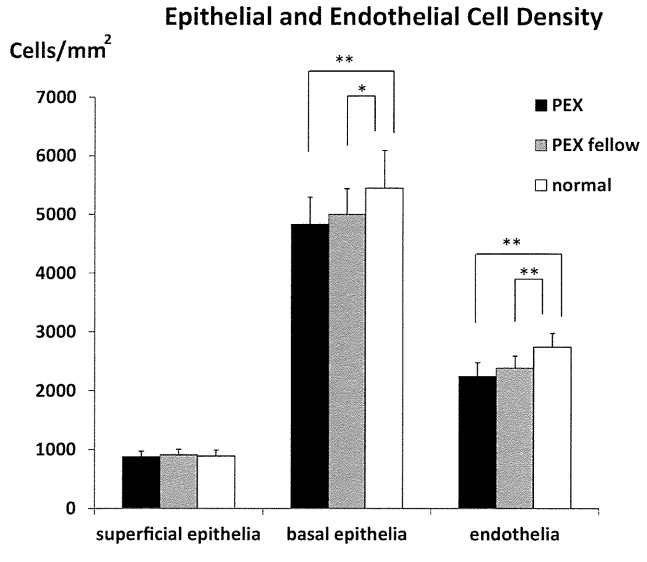

FIGURE 1. Corneal epithelial and endothelial cell densities of eyes with PEX syndrome, their clinically unaffected fellow eyes, and eyes of normal control subjects. $^{**}P < 0.01$; $^{*}P < 0.05$.

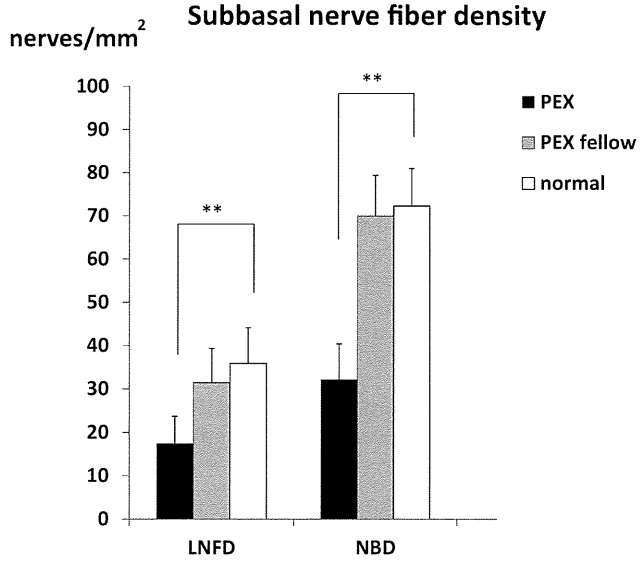

FIGURE 3. Subbasal LNFD and NBD in eyes with PEX syndrome, their clinically unaffected fellow eyes, and eyes of normal control subjects. $^{**}P < 0.01$.

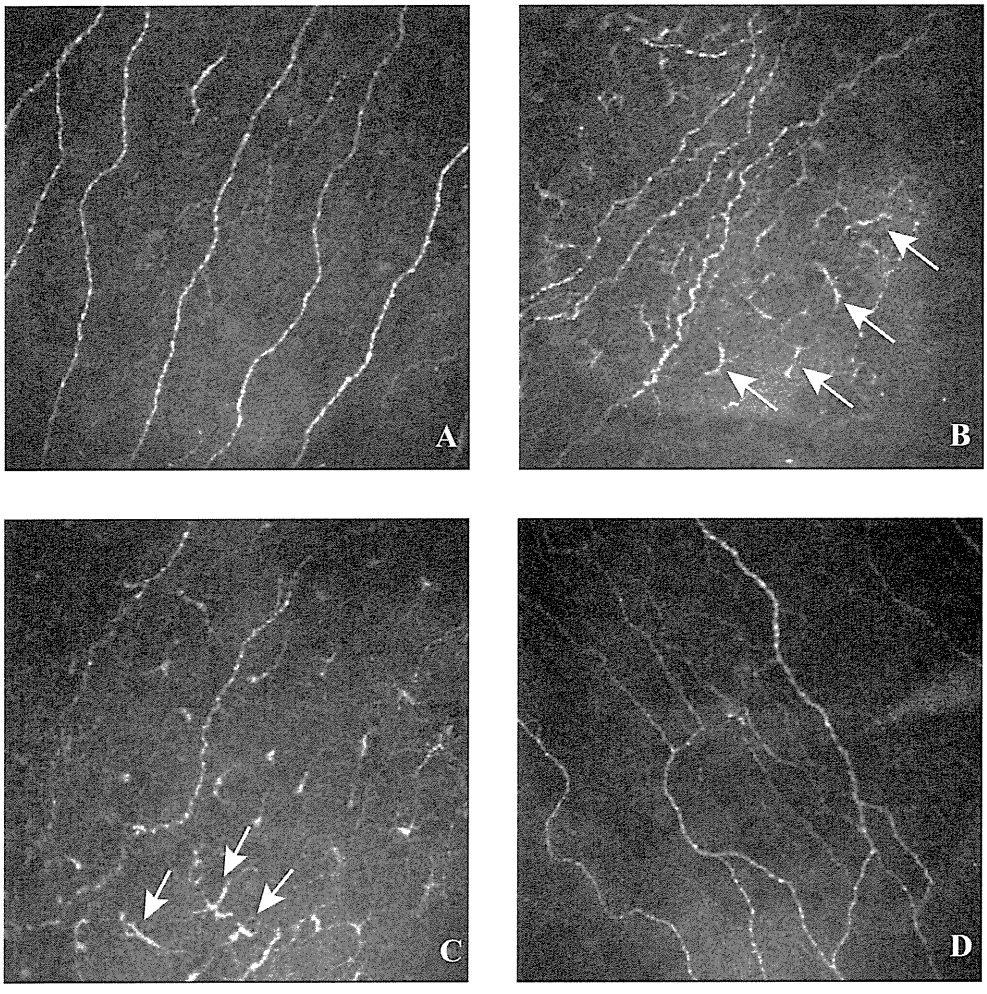

FIGURE 4. In vivo confocal microscopic images of the subbasal nerve plexus in patients with PEX syndrome and a normal control subject. (**A**) Representative image from a normal control subject showing subbasal nerve plexus with long nerve fibers running parallel to the Bowman layer. The nerve fibers appeared to be straight with minimal tortuosity. The subbasal LNFD was 31.3 nerves/mm^2, and the nerve tortuosity was grade 1. (**B**) Representative image from a PEX syndrome eye showing very tortuous nerves with significant convolutions throughout their course. The tortuosity grade was 4. Note the intensive infiltration of dendritic cells (*arrows*) in close vicinity of the nerve fibers. (**C**) Confocal image of the subbasal nerve plexus of another PEX eye showing the thinning of the nerves, short nerve sprouts, fewer branches from the main nerve trunk, and significantly decreased nerve density. The LNFD was 6.3 nerves/mm^2. *Arrows*: dendritic cell infiltration. (**D**) Confocal image of a PEX fellow eye showing moderately tortuous subbasal nerve plexus with a tortuosity grade of 3 and an LNFD of 18.8.

significantly different from those of the controls (31.5 ± 7.8 and 69.9±9.4 nerves/mm^2; $P = 0.093$ and $P = 0.301$).

Confocal images of PEX eyes showed extremely tortuous nerve fibers, thinning of nerves, short nerve sprouts, fewer branches from the main nerve trunk, and highly reflective inflammatory infiltrates in close vicinity of the subbasal nerves. Representative confocal images of the three groups are shown in Figure 4. In PEX eyes, 85.2% (23 of 27 eyes) had grade ≥3 subbasal nerve tortuosity, and the degree of tortuosity in PEX eyes was significantly higher than that of the controls (3.2 ± 0.7 vs. 1.6 ± 0.6; $P < 0.0001$; Wilcoxon rank sum test). The degree of tortuosity in PEX fellow eyes was also greater than that of normal controls, although the difference was not significant (2.1 ± 0.9 vs. 1.6 ± 0.6; $P = 0.054$).

It was our impression that PEX eyes had more inflammatory cells, including dendritic cells, infiltrating the subbasal cell layer and anterior stroma, and these changes were more severe in eyes with decreased subbasal nerve densities and lower corneal sensitivities (Fig. 4).

Correlation between Corneal Sensitivity and Subbasal Nerve Density and Basal Epithelial Cell Density

Spearman's correlation analyses showed that there was a significant positive correlation between corneal sensitivity and the subbasal nerve densities (LNFD, $r = 0.764$, $P < 0.0001$; NBD, $r = 0.634$, $P < 0.0001$; Spearman correlation coefficient). Corneal sensitivity was also significantly and positively correlated with basal epithelial cell density and significantly and negatively correlated with subbasal nerve tortuosity (Table 1).

Confocal Microscopic Detection of Hyperreflective Material

IVCM showed hyperreflective material, probably XFM, in the subbasal epithelial layer or the anterior stroma of 22 of the 27 PEX eyes (81.5%). The hyperreflective material was also observed abundantly in the endothelia of all PEX eyes. Five of 27 (18.5%) PEX fellow eyes showed hyperreflective deposits in the subbasal epithelial layer or anterior stroma, and 14 of 27 (51.9%) had endothelial surface deposits of hyperreflective material. In sharp contrast, none of the normal eyes showed hyperreflective material in the subbasal epithelial or anterior

TABLE 1. Correlation among Corneal Sensitivity, Subbasal Nerve Fiber Density, Tortuosity, and Basal Epithelial Cell Density

	Corneal Sensitivity	
	Spearman Correlation Coefficient	*P*
Long nerve fiber density	0.7640	<0.0001*
Nerve branch density	0.6341	<0.0001*
Subbasal nerve fiber tortuosity	−0.8250	<0.0001*
Basal epithelial cell density	0.6971	<0.0001*

* Statistically significant.

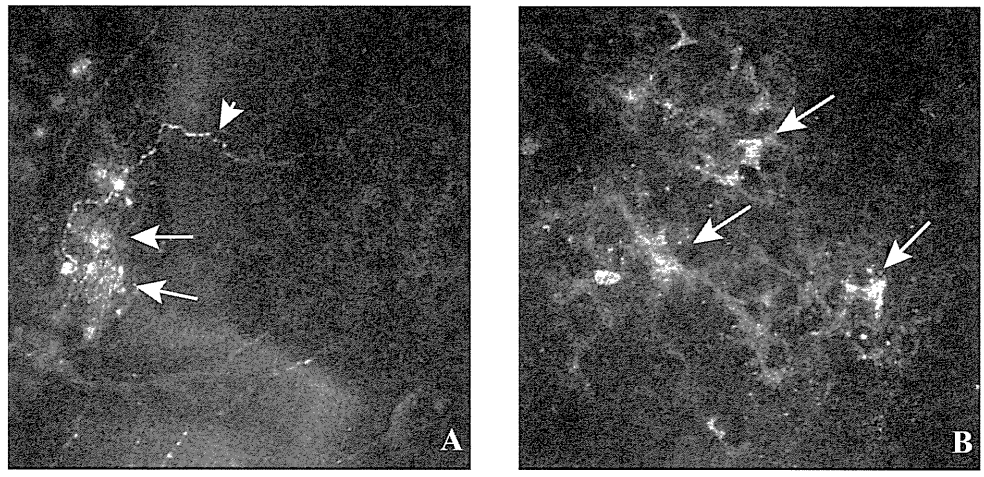

FIGURE 5. Confocal microscopic images showing XFM in the subbasal nerve plexus layer of a patient with PEX syndrome. (**A**) Nerve fiber thinning with tortuous morphology can be seen (*arrowhead*), and XFM (*arrows*) is seen in close vicinity of the pathogenic nerve fibers. (**B**) Hyperreflective deposits (*arrows*) indicative of XFM can be seen in the subbasal amorphous layer of the cornea of another patient in the PEX eye group.

stromal layers, and only two (7.4%) had a small amount of hyperreflective material on the endothelial surface (Figs. 5, 6).

DISCUSSION

The manifestations of PEX syndrome in the anterior segment are widely known to affect intraocular surgery with poor mydriasis and intensive postoperative inflammation. The fact that aggregates of XFM can be identified in autopsy specimens of the heart, lung, liver, kidney, and other organs in patients with ocular PEX suggests that the ocular PEX syndrome is part of a general systemic disorder.[1-3,17] In fact, PEX syndrome has been reported to be associated with cardiovascular diseases, chronic cerebral disorders, Alzheimer disease, and acute cerebrovascular events.[1-3] Two single nucleotide polymorphisms in the lysyl oxidase-like 1 (*LOXL1*) gene have been recently identified as strong genetic risk factors for PEX syndrome and PEX glaucoma.[18]

IVCM with the HRTII-RCM provides a new imaging method that allows rapid, noninvasive, high-resolution, and microstruc-

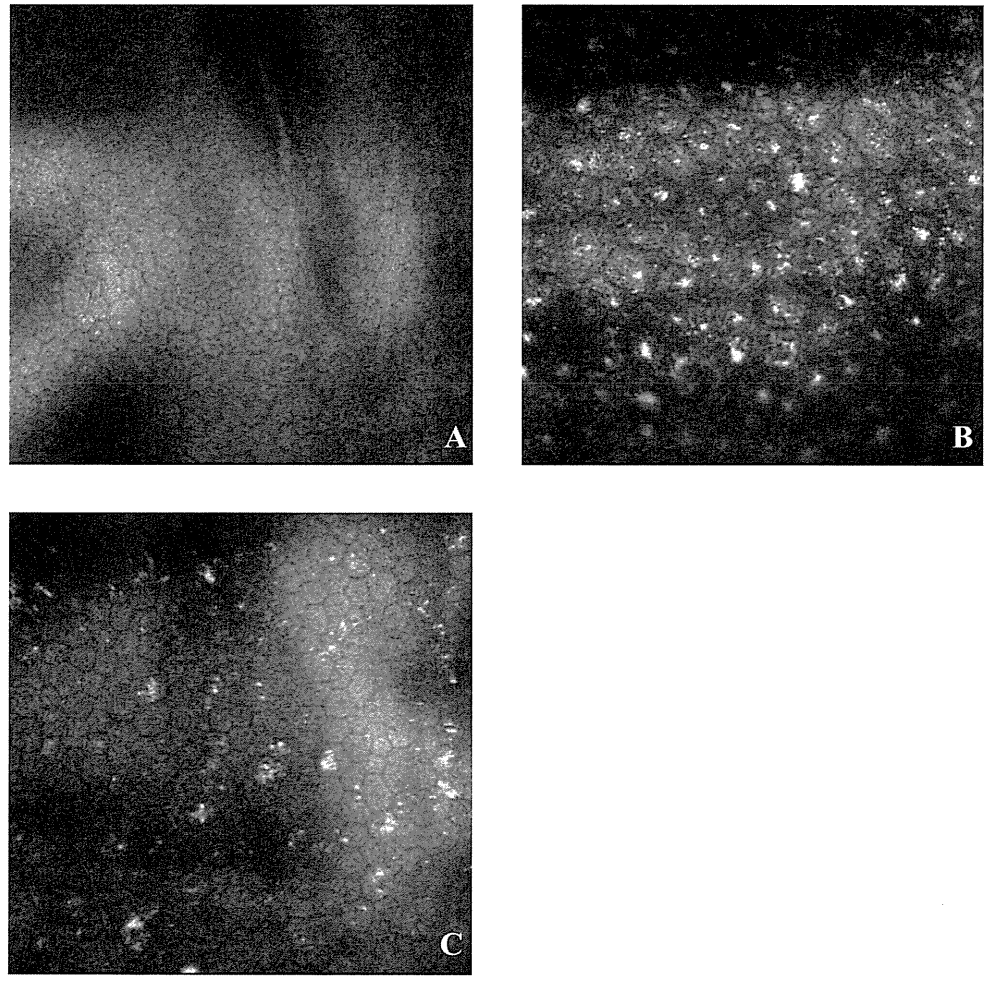

FIGURE 6. Representative confocal microscopic images of the endothelial layers of PEX syndrome eye, PEX fellow eye, and normal control eye group. (**A**) Normal subject with regularly arranged hexagonal endothelial cells. (**B**) PEX eye showing increases in pleomorphism and polymegethism and decrease in cell density. Intense hyperreflective materials indicative of XFM can be seen. (**C**) PEX fellow eye showing similar changes of endothelial cells and deposition of XFM.

tural examination of the cornea.[10,11] Only two studies have used IVCM to study the corneas of patients with PEX syndrome. Martone et al.[12] reported the findings in one case, and they reported that ICVM can detect hyperreflective deposits and dendritic cells infiltrating the basal epithelial cell layer. Fibrillar subepithelial structures were found, and the endothelial layer showed cellular anomalies. In a prospective observational case series, Sbeity et al.[13] used noncontact IVCM to detect XFM on the lens surfaces and corneal endothelia of PEX eyes and their fellow eyes.

Our study was the first to use IVCM to investigate cell densities in different layers of the cornea and to determine alterations of subbasal nerve density and tortuosity in PEX and PEX fellow eyes. Our results showed a significant decrease in the densities of the corneal endothelial cells in PEX eyes and their fellow eyes, which is in agreement with earlier observations by specular microscopy.[8,19,20] In addition, the clear confocal images allowed us to detect pleomorphisms and polymegethisms of the endothelial cells. All PEX eyes and 51.9% of PEX fellow eyes showed deposits of hyperreflective material in the endothelium, indicative of either pigment granules or XFM. In agreement with Sbeity et al.,[13] we believe that the pleomorphic and irregular deposits found on the corneal endothelium most likely represent XFM rather than pigment granules, which are round and uniform in size.[13] In addition, a number of patients who had no visible pigment keratoprecipitates on slit-lamp microscopy were found to have abundant large and irregular hyperreflective deposits on the endothelium in the confocal images.

PEX syndrome–associated corneal endotheliopathy has been suggested to be caused by one or a combination of the following alterations: hypoxic changes in the anterior chamber, accumulation of extracellular matrix, fibroblastic changes of the endothelium, and increased concentration of TGF-β.[1–3] Our confocal microscopic findings suggest that the XFM, possibly at different stages of the normal course of PEX, may be deposited on the endothelium or may migrate from the endothelial cells that undergo fibroblastic changes. Our findings also showed that hyperreflective materials are found not only on the endothelium of PEX eyes but also in their fellow eyes, indicating that the fellow eyes might be at a preclinical stage of PEX syndrome. A bilateral decrease in the endothelial cell counts and morphologic alterations of endothelium support the idea that PEX is a binocular and systemic abnormality. Patients with unilateral PEX syndrome may have asymmetric manifestation of this slowly progressing disease.

Of clinical significance was our finding that the decreased stromal cell densities observed by IVCM could possibly explain the report that the central corneas of PEX eyes were thinner than those of normal subjects.[8] The pathogenesis of the decrease of stromal cell density in PEX eyes warrants future study. Because XFM deposits were simultaneously observed in the anterior stroma of PEX eyes, we suggest that the XFM may be somehow causative for this alteration, perhaps by inducing apoptosis of the keratocytes. Other pathogenic factors, such as altered levels of cytokines or chemokines in the cornea, could also be responsible, and this definitely warrants future investigation. In addition, PEX fellow eyes also had lower cell counts in the stroma, although the difference was not statistically significant. We suggest that the cause of the binocular differences in our study might have been because the two eyes were at different stages of the PEX process, and PEX fellow eyes may still be at a preclinical stage of PEX syndrome.

Other important findings were found in the subbasal nerve plexus. Our results showed that the subbasal nerve density was significantly lower and the nerves were mostly tortuous, with beading and thinning in PEX eyes. Interestingly, PEX fellow eyes also had similar alterations, though the changes were not significant. These findings support the idea that PEX syndrome is a binocular abnormality that is expressed in both eyes but to different degrees. The important clinical significance of our study is that our correlation analyses showed that the decreased subbasal nerve density and increased tortuosity were significantly correlated with decreased corneal sensitivity. These results provide evidence, for the first time, that the cause of the decreased corneal sensitivity in eyes with PEX syndrome is the decreased subbasal nerve density. For patients with PEX syndrome, it would be practical and feasible to examine corneal sensitivity to assess the severity of PEX keratopathy and perhaps to predict the progression of PEX syndrome. In addition, detection of the morphologic changes in cell densities and subbasal nerve abnormalities by IVCM in the fellow eyes indicates that it is a sensitive tool for the diagnosis of preclinical stage of PEX syndrome. Our findings showed that PEX keratopathy may develop before any clinically visible XFM deposits are detected on the lens capsule or iris. If these findings are confirmed, then keratopathy may be the first event of the ocular complications of PEX syndrome. These findings also indicate that clinically unaffected fellow eyes of patients with PEX syndrome are probably at risk for PEX syndrome, and more frequent ophthalmologic examinations are necessary.

This study has increased our understanding of the keratopathy of this most likely systemic abnormality. Whether the alternations of the subbasal corneal nerves are primary or secondary changes of the disease must be determined. Because of the increase in the elastic microfibril components and imbalances in the matrix metalloproteinases (MMPs) and tissue inhibitors of MMP in eyes with PEX syndrome, PEX fibrils accumulate in the tissues.[1–3] Our findings that XFM deposits were frequently observed close to the subbasal epithelial layer or anterior stroma support the idea that besides an abnormal aggregation of elastic microfibrils into exfoliation fibers (the elastic microfibril hypothesis),[1–3,21] other extracellular matrix components, such as basement membrane components, may possibly interact and become incorporated into the composite XFM (the basement membrane hypothesis).[2,3] In addition, our observation of an infiltration of dendritic cells in close vicinity of the subbasal nerve plexus layer indicates the possibility that accumulation of extracellular XFM may induce inflammatory responses, which then recruit antigen-presenting cells such as immunocompetent dendritic cells. This excessive deposition of XFM and infiltration of dendritic cells may play a role in the neuropathy of the subbasal nerve plexus, resulting in decreased corneal sensitivity in patients with PEX syndrome.

Some limitations were present this study. First, the IVCM scans a very small area of the cornea, which may generate biases among different portions of scanning of different groups. As mentioned, efforts were taken to scan the center of the cornea of each subject. In addition, we also confirmed our findings by scanning the midperipheral and peripheral portions of the cornea (data not shown).

Second, IVCM images may not represent the true histologic changes of the cornea. By applying the same criteria for image evaluation, we can conclude that the differences between the studied groups were still detected. Furthermore, it was our impression that fewer keratocytes were seen in the stromas of corneal specimens obtained from PEX syndrome patients with penetrating keratoplasty.

Future investigations, including a thorough and quantitative analysis of the exfoliation material by confocal imaging, are needed. In addition, the correlations between IVCM findings with endothelial barrier function should be determined. If the confocal findings can provide clues for preclinical stages of endothelial barrier dysfunction of the cornea in PEX syndrome, their clinical significance can be used in designing an early treatment protocol.

In summary, our study demonstrated that eyes with PEX syndrome have decreased cell densities in the cornea. The subbasal nerve density was also significantly decreased, and this was significantly correlated with clinically decreased corneal sensitivity. Our study sheds light on understanding the cause of impaired corneal sensitivity in patients with PEX syndrome. The PEX syndrome is probably a bilateral event in which the keratopathy of the fellow eye also must be observed.

References

1. Naumann GOH, Schlötzer-Schrehardt U, Kuchle M. Pseudoexfoliation syndrome for the comprehensive ophthalmologist: intraocular and systemic manifestations. *Ophthalmology.* 1998;105:951-968.
2. Schlötzer-Schrehardt U, Naumann GOH. Ocular and systemic pseudoexfoliation syndrome. *Am J Ophthalmol.* 2006;141:921-937.
3. Ritch R, Schlötzer-Schrehardt U. Exfoliation syndrome. *Surv Ophthalmol.* 2001;45:265-315.
4. Forsius H. Prevalence of pseudoexfoliation of the lens in Finns, Lapps, Icelanders, Eskimos, and Russian. *Trans Ophthalmol Soc UK.* 1979;99:296-298.
5. Naumann GOH, Schlötzer-Schrehardt U. Keratopahty in pseudoexfoliation syndrome as a cause of corneal endothelial decompensation—a clinicopathologic study. *Ophthalmology.* 2000;107:1111-1124.
6. Abbott RL, Fine BS, Webster RB Jr, et al. Specular microscopic and histologic observations in nonguttata corneal endothelial degeneration. *Ophthalmology.* 1981;88:788-800.
7. Detorakis ET, Koukoula S, Chrisohoou F, Konstas AG, Kozobolis VP. Central corneal mechanical sensitivity in pseudoexfoliation syndrome. *Cornea.* 2005;24:688-691.
8. Inoue K, Okugawa K, Oshika T, Amano S. Morphological study of corneal endothelium and corneal thickness in pseudoexfoliation syndrome. *Jpn J Ophthalmol.* 2003;47:235-239.
9. Kozobolis VP, Christodoulakis EV, Naoumidi II, Siganos CS, Detorakis ET, Pallikaris LG. Study of conjunctival goblet cell morphology and tear film stability in pseudoexfoliation syndrome. *Graefes Arch Clin Exp Ophthalmol.* 2004;242:478-483.
10. Patel DV, McGhee CNJ. In vivo confocal microscopy of human corneal nerves in health, in ocular and systemic disease, and following corneal surgery: a review. *Br J Ophthalmol.* 2009;93:853-860.
11. Guthoff RF, Zhivov A, Stachs O. In vivo confocal microscopy, an inner vision of the cornea—a major review. *Clin Exp Ophthalmol.* 2009;37:100-117.
12. Martone G, Casprini F, Traaversi C, Lepri F, Picherri P, Caporossi A. Pseudoexfoliation syndrome: in vivo confocal microscopy analysis. *Clin Exp Ophthalmol.* 2007;35:582-585.
13. Sbeity Z, Palmiero PM, Tello C. Liebmann JM, Ritch R. Non-contact in vivo confocal scanning laser microscopy in exfoliation syndrome, exfoliation syndrome suspect and normal eyes. *Acta Ophthalmol.* 2009 Oct 23 [Epub ahead of print].
14. Hu Y, Matsumoto Y, Adan ES, et al. Corneal in vivo confocal scanning laser microscopy in patients with atopic keratoconjunctivitis. *Ophthalmology.* 2008;115:2004-2012.
15. Quadrado MJ, Popper M, Morgado AM, Murta JN, Best JAV. Diabetes and corneal cell densities in humans by in vivo confocal microscopy. *Cornea.* 2006;25:761-768.
16. Mocan MC, Durukan I, Irkec M, Orhan M. Morphologic alterations of both the stromal and subbasal nerves in the corneas of patients with diabetes. *Cornea.* 2006;25:769-773.
17. Schlötzer-Schrehardt U, Koca M, Naumann GOH, Volkholz H. Pseudoexfoliation syndrome: ocular manifestation of a systemic disorder? *Arch Ophthalmol.* 1992;110:1752-1756.
18. Thorleifsson G, Magnusson KP, Sulem P, et al. Common sequence variants in the LOXL1 gene confer susceptibility to exfoliation glaucoma. *Science.* 2007;317:1397-1400.
19. Wang L, Yamasita R, Hommura S. Corneal endothelial changes and aqueous flare intensity in pseudoexfoliation syndrome. *Ophthalmologica.* 1999;213:318-391.
20. Miyake K, Matsuda M, Inaba M. Corneal endothelial changes in pseudoexfoliation syndrome. *Am J Ophthalmol.* 1989;108:49-52.
21. Streeten BW, Gibson SA, Dark AJ. Pseudoexfoliative material contains an elastic microfibillar-associated glycoprotein. *Trans Am Ophthalmol Soc.* 1986;84:304-320.

Anterior Segment Optical Coherence Tomography Analysis of Clinically Unilateral Pseudoexfoliation Syndrome: Evidence of Bilateral Involvement and Morphologic Factors Related to Asymmetry

Xiaodong Zheng,[1] *Hiroshi Sakai,*[2] *Tomoko Goto,*[1,3] *Koji Namiguchi,*[1] *Shiro Mizoue,*[1] *Atsushi Shiraishi,*[1] *Shoichi Sawaguchi,*[2] *and Yuichi Ohashi*[1]

Purpose. To compare the morphology of the anterior chamber angle (ACA) and iris in eyes with pseudoexfoliation (PEX) syndrome to that of their clinically unaffected fellow eyes and normal control eyes.

Methods. Forty-two patients with unilateral PEX syndrome and 42 normal subjects were studied. Eyes were separated into those with PEX, their clinically unaffected fellow eyes, and normal eyes. The dark-light changes of the ACA and iris were documented by anterior segment optical coherence tomography (AS-OCT) video recordings. The nasal ACA parameters including the angle opening distance at 500 μm (AOD500), the trabecular-iris space at 500 μm (TISA500), and the trabecular-iris angle at 500 μm (TIA500); anterior chamber depth (ACD); iris-lens contact distance (ILCD), and iris configuration were analyzed with the built-in software and a customized program.

Results. The ACA parameters were not significantly different among all three groups in the dark. The PEX eyes had significantly smaller ACA parameters than their fellow eyes and normal control eyes in the light. PEX eyes also had significantly shallower ACD, longer ILCD, and greater iris convexity (both in dark and light), and thinner iris (in dark) than their fellow eyes. The fellow eyes had significantly lower ACD both in the dark and light, and smaller angle opening distance at 500 μm and ILCD in the light than normal controls. There were no significant differences in the iris area among the three groups.

Conclusions. Differences in the anterior segmental morphology are present between PEX and fellow eyes. These disparities may be related to the asymmetry in patients with the unilateral PEX syndrome. (*Invest Ophthalmol Vis Sci.* 2011;52:5679–5684) DOI:10.1167/iovs.11-7274

The pseudoexfoliation (PEX) syndrome is a common age-related disorder of the extracellular matrix that can affect 10%–20% of people older than 60 years worldwide.[1,2] The main ocular manifestation of PEX is the production and progressive accumulation of abnormal extracellular fibrillar and pseudoexfoliation material in almost all of the inner walls of the anterior segment of the eye. There has been a renewed interest in this disease because of the better awareness of the complications accompanying PEX including phacodonesis and lens subluxation, intractable glaucoma, melanin dispersions, poor mydriasis, blood-aqueous barrier dysfunction, and posterior synechiae.[1,2]

Up to 76% of patients with PEX are initially diagnosed as having unilateral PEX.[3] However in an electron microscopic study, Parekh et al. reported that 26 of 32 patients (81%) with clinically unilateral PEX had pseudoexfoliation material on either the lens capsule or conjunctival samples of the clinically unaffected eyes.[4] Furthermore, several reports on the follow-up of patients with unilateral PEX documented that 74% to 81.6% of the unilateral cases became bilateral.[5–7] This suggested that unilateral PEX is in fact a bilateral but asymmetric condition, and the percentage of unilateral disease decreases with a corresponding increase in bilateral disease with increasing age. The factors affecting the conversion from unilateral to bilateral disease are not known, and the pathogenic mechanism underlying the asymmetric condition has not been determined. Subtle differences in ocular blood flow,[8] aqueous humor dynamics, blood-aqueous barrier function, or anterior segmental morphology might be responsible for the asymmetry.[1,2]

Ultrasound biomicroscopic (UBM) studies on the morphologic alterations of the anterior segment of PEX eyes have shown abnormalities of the zonules, lens thickening, shallow central anterior chamber depth (ACD), and occludable angles.[9–14] In unilateral PEX patients, the PEX eyes and fellow eyes have been reported to share some similar morphologic changes.[14]

With the advancement of ophthalmic imaging instruments, more information has been obtained on the morphology of the structures in different ocular disorders. Fourier domain anterior segment optical coherence tomography (AS-OCT) is a representative imaging technique that provides cross-sectional views of the anterior segment with a resolution better than that of UBM.[15] Images and measurements of very fine structures can be achieved rapidly and noninvasively. In addition, using the AS-OCT video mode has allowed investigators to document dynamic morphologic alterations of the anterior chamber angle (ACA) and iris during pupillary movements without being influenced by accommodation.[16–18]

The purpose of this study was to compare the morphology of the anterior segment of affected eyes and their fellow eyes in cases of unilateral PEX. To accomplish this, we recorded images of the anterior segment by AS-OCT during pupillary dilation and constriction. Comparisons were made of the ACA

From the [1]Department of Ophthalmology, Ehime University School of Medicine, Toon City, Ehime, Japan; [2]Department of Ophthalmology, University of the Ryukyus Hospital, Okinawa, Japan; and [3]Department of Ophthalmology, Takanoko Hospital, Matsuyama, Ehime, Japan.

Submitted for publication January 25, 2011; revised March 16, 2011; accepted April 19, 2011.

Disclosure: **X. Zheng**, None; **H. Sakai**, None; **T. Goto**, None; **K. Namiguchi**, None; **S. Mizoue**, None; **A. Shiraishi**, None; **S. Sawaguchi**, None; **Y. Ohashi**, None

Corresponding author: Xiaodong Zheng, Department of Ophthalmology, Ehime University School of Medicine, Ehime 791-0295, Japan; xzheng@m.ehime-u.ac.jp.

and the iris parameters in the PEX eyes, their fellow eyes, and normal control eyes.

Subjects and Methods

Patients and Control Subjects

We studied 45 consecutive patients with unilateral PEX syndrome who visited the Department of Ophthalmology, Ehime University from January 2009 to November 2010. All eyes were examined by slit-lamp biomicroscopy after pupillary dilation. PEX eyes had clinically evident PEX material at the pupillary border or on the anterior lens capsule in one eye. These eyes were placed in the PEX eye group. Their clinically unaffected fellow eyes were placed in the fellow eye group. Forty-five age- and sex-matched normal subjects were also studied and one eye was randomly selected as the normal control.

The exclusion criteria included: prior intraocular surgery, e.g., laser trabeculoplasty, laser iridotomy, laser iridoplasty, or ocular trauma; evidence of peripheral anterior synechiae on indentation; iris dystrophy or dyscoria; lymphoma, sarcoidosis, diabetic mellitus, inflammation; eyes using anti-glaucoma medications or having abnormal intraocular pressure; or use of systemic medications that could affect the ACA or pupillary reflex.

All participants underwent a complete ophthalmic examination, including best-corrected visual acuity, autorefraction, slit-lamp microscopy, and intraocular pressure measurements by applanation tonometry (Goldmann; Haag-Streit, Köniz, Switzerland). The ocular axial length was measured (IOL Master; Carl Zeiss, Jena, Germany). Gonioscopy was performed with a 4-mirror lens at high magnification (×16) with the eye in the primary position of gaze. All investigated eyes had open-angles and all structures anterior to the scleral spur were identified by gonioscopy (Shaffer grade ≧ 2).

The procedures used conformed to the tenets of the Declaration of Helsinki. An informed consent was obtained from all subjects after an explanation of the nature and possible consequences of the procedures. The protocol used was approved by the Ethics Committee of Ehime University School of Medicine.

Anterior Segment Optical Coherence Tomography

An experienced operator who was masked to the results of the ophthalmic examinations performed the AS-OCT (Swept-source 1000 CASIA AS-OCT, Tomey, Nagoya, Japan). This AS-OCT system had a 30 kHz axial scan rate with an axial resolution of 10 μm. The use of 1310 nm wavelength coupled with high resolution Fourier domain-OCT improved the resolution and penetration of the measuring beam into turbid tissues with a scan depth of 6 mm. This was sufficient to image the entire anterior segment in one frame.[15] The scan of the anterior chamber was a noncontact procedure during which the subject fixated on an internal target.

The AS-OCT real-time video recording mode (4 frames per second) was used to study the changes of the ACA and the iris during pupillary dilation and light-induced constriction. The scan was centered on the pupil, and the scan passed along the nasal-temporal axis, i.e., 0° to 180°. After one minute at 50 lux of dark-adaptation, a LED pen light (Gentos, Tokyo, Japan), fixed at a distance of 20 cm, 45° from the optic axis of the examined eye, was turned on. The illuminance of the light was standardized at 2000 lux, and it was kept on for 4 seconds to induce pupillary constriction. AS-OCT scans were recorded for 10 seconds and the operator chose the best video frame with good centering to analyze. Data were excluded if the scleral spur could not be identified or the frame was of suboptimal quality because of blinks and eye movements. Each eye was examined three times with an intertest interval of at least 10 minutes.

Image Processing

All images were processed separately and analyzed by two observers (XZ and KN) who were masked to the clinical findings of the eye. The video file was reviewed and one frame of the images in the dark (most dilated pupil) and the light (most constricted pupil) were selected for each subject. The morphology of structures on the nasal side of the eye was analyzed. Images were first analyzed with the built-in software for the ACA parameters: angle opening distance at 500 μm (AOD500), trabecular-iris space at 500 μm (TISA500), and trabecular-iris angle at 500 μm (TIA500). The central anterior chamber depth (ACD) and the pupillary diameter were also measured (Fig. 1A).

All images were then exported and analyzed with a customized software program written for the following iris parameters (Fig. 1B): the iris thickness in the dilator muscle region (DMR) which was set at one-half of the distance between the scleral spur and the pupillary margin was measured as described[19]; and the iris thickness in the sphincter muscle region (SMR) which was set at 0.75 mm from the pupillary margin was also measured. The ratio of the thickness at

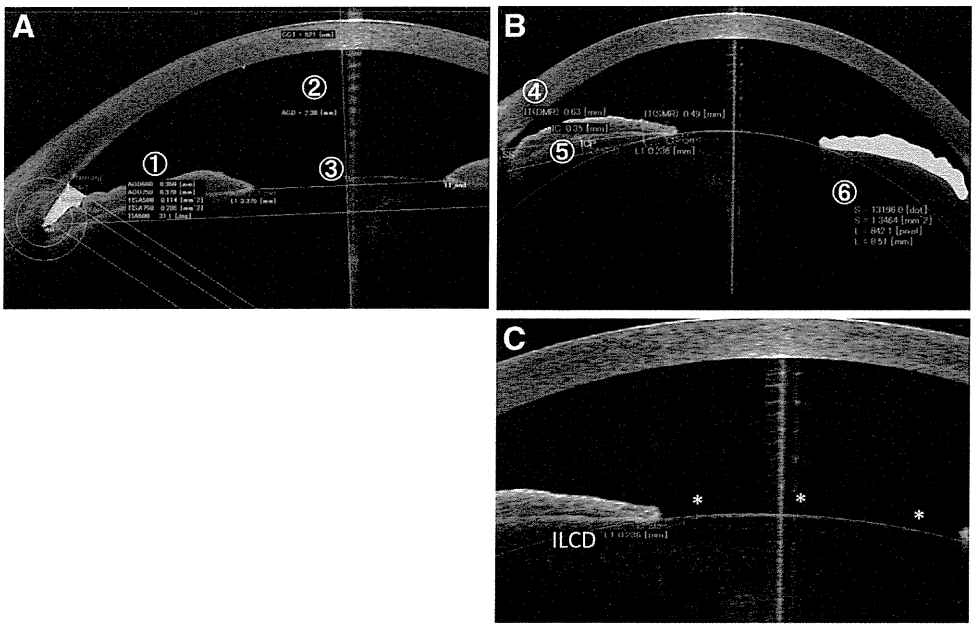

Figure 1. Anterior segment optical coherence tomographic (AS-OCT) images from which the morphologic parameters of the structures in the anterior chamber and the iris were measured. (**A**) Anterior chamber parameters of (1) angle measurements (AOD500, TISA500, and TIA500 were used), (2) central anterior chamber depth (ACD), and (3) pupillary diameter. (**B**) Iris configurations of (4) iris thickness (IT) at the dilator muscle region (DMR) measured at one-half of the distance between the scleral spur (SS) and the pupillary margin; iris thickness at the sphincter muscle region (SMR) measured at 0.75 mm from the pupillary margin, (5) iris convexity (IC), and (6) iris area (indicated by *green shading* over the right half of the iris). (**C**) Iris-lens contact distance (ILCD) measurement. *Asterisks* represent three points selected on the lens surface for generating estimated curved line of the anterior lens capsule. The ILCD was measured along the iris pigment epithelium from the papillary border to the point at which the iris was seen to separate from the anterior lens capsule.

the DMR and SMR (DMR/SMR) was used for the statistical analyses to reduce the intersubject variability.

In addition, the iris convexity was defined as the distance between the posterior point of greatest iris curvature to a line drawn from the most peripheral to the most central points of the iris pigment epithelium. The area of the iris was determined by the cumulative cross-sectional area of the iris from the scleral spur to the edge of the pupil.[20] A program was also written for the calculation of iris-lens contact distance (ILCD). To measure this, 3 points were manually designated on the lens surface and a curved line of the anterior lens capsule was automatically generated by the software. The ILCD was measured along the iris pigment epithelium from the pupillary border to the point at which the iris was seen to separate from the anterior lens capsule (Fig. 1C). These measurements had good reliability with the intraobserver and interobserver intraclass correlation coefficients ranging between 0.96 to 0.98 and 0.97 to 0.99, respectively.

Statistical Analyses

All data are expressed as the means ± standard deviations (SDs). Gender differences between PEX patients and normal subjects were evaluated by the χ^2 test. Comparisons of other demographic data, biometric characteristics, and AS-OCT parameters were evaluated by paired *t*-tests (PEX eye versus fellow eye) or two-tailed Student's *t*-tests (PEX eye versus normal control eye or fellow eye versus normal control eye). The ACA and iris parameters were compared with adjustment for pupil size. The significance of the differences in the DMR/SMR ratio among the three groups was determined by the Tukey-Kramer test. A probability level of $P < 0.05$ was considered statistically significant. Data were analyzed with statistical software (JMP version 9.0 for Windows; SAS Japan Inc., Tokyo, Japan).

Results

Three patients with unilateral PEX and three normal subjects were excluded due to a poor imaging of the scleral spur. Forty-two patients (17 men and 25 women with a mean age of 72.7 ± 7.4 years and a range of 61 to 92 years) and 42 normal subjects (16 men and 26 women with a mean age of 73.6 ± 8.9 years and a range of 64 to 90 years) were analyzed. The mean age of the PEX patients was not significantly different from that of the normal controls ($P = 0.886$, two-tailed Student's *t*-test). Slit-lamp biomicroscopy showed that all eyes with PEX had typical whitish exfoliation material at the pupillary edge and on the anterior lens capsule. The fellow eyes and normal control eyes did not have these deposits. The differences in the visual acuity, gender distribution, refractive error (spherical equivalent), axial length, intraocular pressure, and gonioscopic grading (Shaffer) of the ACA among the three groups were not significant. The data are summarized in Table 1.

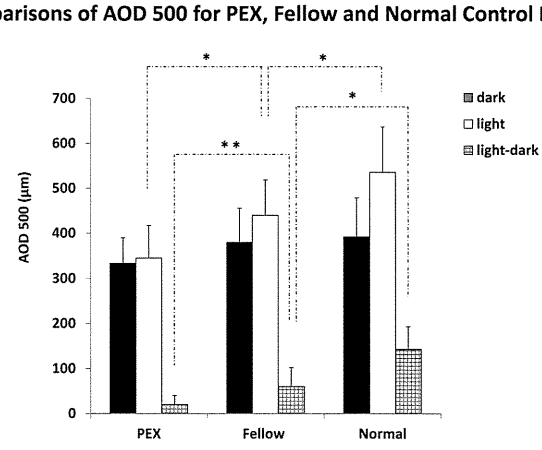

Figure 2. Comparisons of AOD500 for eyes with the PEX syndrome, their unaffected fellow eyes, and normal control eyes. Dark, values measured in the dark when pupils were mostly dilated; Light, values measured in the light when pupils were mostly constricted; Light-dark, $AOD500_{(light)} - AOD500_{(dark)}$. Statistical significance is denoted by $^{**}P < 0.01$, and $^{*}P < 0.05$.

Anterior Chamber Angle (ACA) Morphology

In the dark when pupils were dilated, the mean AOD500 was 333.6 ± 56.5 μm in the PEX eyes, 380.1 ± 76.4 μm in the fellow eyes, and 392.6 ± 87.2 μm in the normal control eyes (Fig. 2). The differences between the three groups were not significant (PEX versus fellow, $P = 0.225$, paired *t*-tests; PEX versus normal, $P = 0.133$; and fellow versus normal, $P = 0.416$, both two-tailed Student's *t*-test). When the pupils were constricted by light, the AOD500 in the PEX eyes was significantly smaller than that of the fellow eyes ($P = 0.021$) and the normal eyes ($P = 0.008$). The AOD500 in the fellow eyes was also significantly smaller than that of the normal eyes ($P = 0.037$). In addition, the mean dark-to-light change of the AOD500 for the PEX eyes was also significantly less than that of the fellow eyes (20.5 ± 16.6 μm vs. 60.8 ± 42.2 μm; $P = 0.007$) and of the normal control eyes ($P = 0.004$). The difference in the changes of the AOD500 between the fellow and normal control eyes was also significant ($P = 0.033$).

In the dark, the TISA500 was not significantly different among the three groups. However in light, the TISA500 of the PEX eyes was significantly smaller than that of the fellow eyes and normal control eyes (Fig. 3).In the light, the PEX eyes also had significantly narrower TIA500 than that of the fellow and normal control eyes. Similarly, the dark-to-light change of the TIA500 of the PEX eyes was significantly less than that of the

Table 1. Demographic and Biometric Characteristics of PEX Eye, Fellow Eye, and Normal Control Eye Groups

	PEX	Fellow	Normal	*P*
Age, y	72.7 ± 7.4	—	73.6 ± 8.9	0.886*
Sex, male/female	17/25	—	16/26	0.763†
Spherical equivalent, D	−0.34 ± 2.8	−0.22 ± 1.76	−0.28 ± 1.52	0.521‡
BCVA, LogMAR	0.04 ± 0.05	0.03 ± 0.04	0.00 ± 0.03	0.554‡
Axial length, mm	23.71 ± 0.94	24.06 ± 0.81	24.5 ± 1.01	0.669‡
Intraocular pressure, mm Hg	14.8 ± 3.1	13.6 ± 3.8	13.1 ± 4.8	0.375‡
Gonioscopy grading (Shaffer)	2.9 ± 0.68	3.1 ± 0.77	3.1 ± 0.82	0.428‡

Data are given as mean ± SD. All groups, $n = 42$. BCVA, best-corrected visual acuity; D, Diopter; LogMAR, logarithm of the minimum angle of resolution.

* PEX patients versus normal control subjects (two-tailed Student's *t*-test).

† PEX patients versus normal control subjects (χ^2).

‡ PEX eye versus fellow eye (paired *t*-test).

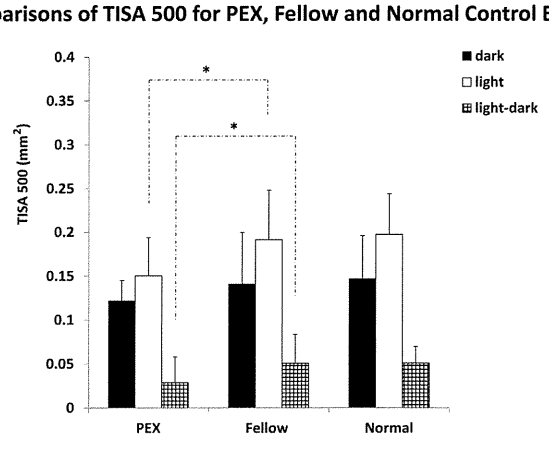

FIGURE 3. Comparisons of TISA500 for eyes with the PEX syndrome, their unaffected fellow eyes, and normal control eyes. Dark, values measured in the dark when pupils were mostly dilated; Light, values measured in the light when pupils were mostly constricted; Light-dark, $TISA500_{(light)} - TISA\ 500_{(dark)}$. Statistical significance is denoted by $^{*}P < 0.05$.

fellow eyes (Fig. 4). The PEX eyes had significantly smaller ACD than that of the fellow eyes both in dark and light ($P = 0.021$ and $P = 0.018$, respectively; paired t-tests; Table 2). The ACD of the fellow eyes was also significantly smaller than that of normal control eyes ($P = 0.038$ and $P = 0.032$ for dark and light respectively; two-tailed Student's t-test).

The pupillary diameter in dark for the PEX eyes was significantly smaller than that of fellow eyes ($P = 0.011$). When the dark-to-light change was analyzed, the PEX eyes had significantly less pupillary change than that of the fellow eyes ($P = 0.025$) and the normal control eyes ($P = 0.008$).

Iris Configuration

The difference in the area of the iris was not significant among the three groups either in dark or light. The mean iris convexity of the PEX eyes was 286.3 ± 63.7 μm in the dark and 251.5 ± 72.4 μm in the light. The mean iris convexity of the fellow eyes was 239.4 ± 86.6 μm in the dark and 195.1 ± 59.3 μm in the light. The iris convexity was significantly greater in the PEX eyes than that of their fellow eyes both in the dark and the light ($P = 0.029$ and $P = 0.038$, respectively; paired t-tests). The convexity of the iris of the fellow eyes was also larger than that of the normal controls but the difference was not significant.

The DMR/SMR ratio in dark for PEX eyes was significantly less than that of the fellow eyes ($P = 0.037$; Tukey-Kramer test). The differences in the DMR/SMR ratio among the three groups in light were not significant (Table 2).

Iris-Lens Contact Distance (ILCD)

The mean ILCD of PEX eyes was 0.523 ± 0.14 mm in the dark and 0.908 ± 0.15 mm in the light. The mean ILCD of the fellow eyes was 0.346 ± 0.12 mm in the dark and 0.732 ± 0.11 mm in the light. The differences in the ILCD between PEX and fellow eyes were significant both in dark and light ($P < 0.001$ for both; paired t-tests; Figure 5). In the light, the ILCD of the fellow eyes was also significantly longer than that of normal control eyes ($P = 0.035$; two-tailed Student's t-tests; Fig. 5).

DISCUSSION

Our findings showed that AS-OCT can be used for noninvasive, quantitative, and reliable analyses of the ACA and iris morphology in eyes with the PEX syndrome. These findings would probably not be obtained by regular gonioscopy or slit-lamp examination. Analyzing the video files provided us with a useful method to accurately examine the ACA and iris configuration when the pupil was most dilated or constricted. This then allowed us to detect subtle changes between the dark and light conditions.

The differences in the ACA parameters, namely, the AOD500, TISA500, and TIA500, among the three groups were not significant in the dark. However, when the pupil was constricted by light, the PEX eyes had significantly smaller values for all the ACA parameters indicating that the widening of the ACA was significantly more impaired in PEX eyes than in their fellow eyes or normal controls. These findings combined with the smaller ACD in PEX eyes indicate the possibility of a weakness of the zonular fibers and forward shifting of the lens, which is consistent with the previous UBM studies.[10–14] For our PEX patients, although the lens shifting was too small to cause a statistically significant change in the refraction, this alteration could be detected by the highly sensitive AS-OCT analysis.

It is known that melanin granules derived from the iris pigment epithelium and PEX deposits form posterior synechiae starting from the early stages of the PEX process.[1,2] These morphologic changes may account for the poor mydriasis, increased iridolenticular contact, and decreased ability of ACA widening during pupillary constriction.

On the other hand, these morphologic alterations may be pathogenic factors for PEX development or the cause for PEX progression in the PEX process. The morphologic changes may also lead to decreased blood flow or circulatory disturbances resulting in abnormalities in the microenvironment of the anterior chamber such as hypoxia and elevation of cellular stress.[1,2,8] Increased pathologic cytokine or chemokine levels, hypoxic conditions, and circulatory factors in the anterior segment of the eye may also play pivotal roles in the progression of PEX. The relationships among these factors with the morphologic changes need to be investigated.

The iris-lens contact distance (ILCD) was also compared among the three groups. Although ultrasound microscopy can be used for direct measurements of ILCD,[21–23] our study provided a rapid, noncontact method in evaluating this parameter by AS-OCT imaging. The use of Fourier domain AS-OCT provided excellent images of the iris configuration and in combi-

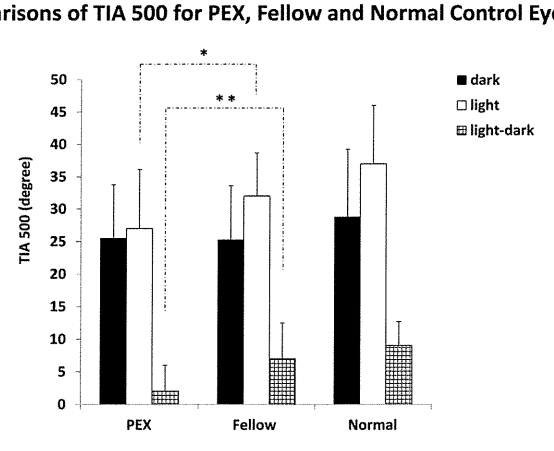

FIGURE 4. Comparisons of TIA500 for eyes with the PEX syndrome, their unaffected fellow eyes, and normal control eyes. Dark, values measured in the dark when pupils were mostly dilated; Light, values measured in the light when pupils were mostly constricted; Light-dark, $TIA500_{(light)} - TIA500_{(dark)}$. Statistical significance is denoted by $^{**}P < 0.01$, and $^{*}P < 0.05$.